RSC Advances

Thermal Behavior of Long-chain Alkanoylcholine Soaps

Ainhoa Tolentino,[1] Abdelilah Alla,[1] Antxon Martínez de Ilarduya,[1]
Mercè Font-Bardia,[2] Salvador León,[3] and Sebastián Muñoz-Guerra[1]*

[1]*Departament d'Enginyeria Química, Universitat Politècnica de Catalunya, ETSEIB, Diagonal 647, Barcelona 08028, Spain.*

[2]*Centre Cientific i Tecnològic (CCiTUB), Universitat de Barcelona, Sole Sabaris 1-3, Barcelona 08028, Spain.*

[3]*Departmento de Ingeniería Química, Universidad Politécnica de Madrid, ETSIIM, Gutierrez Abascal 2, Madrid 28006, Spain.*
E-mail: sebastian.munoz@upc.edu

Long-chain alkanoylcholines prepared from fatty acids (*n*ACh) are fully sustainable cationic surfactants that are known for their biological and medicinal properties. In the present work the thermal behavior of the homologous series of alkanoylcholine iodides with *n* =12, 14, 16 and 18, has been examined along the 25-200 ºC range of temperatures. Up to three thermotropic phases have been identified, and the thermal transitions implied in their interconversion have been characterized by DSC and simultaneous WAXS and SAXS analysis carried out in real-time. The all three phases consist of a bilayered structure with alkanoyl chains confined in the space between the head group layers and interdigitated in a more or less extent. Melting-crystallization of either the polymethylene segments or the choline iodide groups is involved in such transitions. Additionally, a crystal phase consisting also of a bilayered structure but excluding side chain interdigitation was observed upon crystallization from solution and its structure was elucidated by single-crystal X-ray diffraction direct methods. The close correlation existing between thermal properties, phase structure and *n* has been brought into evidence.

Introduction

Choline derivatives are extensively investigated due to multiple reasons. Choline itself, (2-hydroxyethyl)trimethyl ammonium salt, is a naturally occurring compound of extreme biological relevance as precursor of neurotransmissors and membrane constituents.[1,2] Choline is biocompatible and able to biodegrade both in living organisms[3] and in the environment,[4] a faculty that makes their derivatives very promising candidates for the preparation of sustainable eco-friendly materials. Such behavior has in fact incentivized the use of choline as additive for eutectic solvents[5] or as counter-ion in ionic liquids, to which it is able to bring down their melting points.[6] On the other hand, choline based ionic surfactants are distinguished by displaying low Krafft temperatures.[7,8] Recent works have shown that it is possible to have green surfactants with good water solubility from long-chain alkanoates by using choline as counterion.[9]

1

The work reported in this paper is related to the use of choline in the design of surfactants derived from fatty acids. The thermotropic behavior of alkanoate soaps has been studied in detail for long time.[10] It is well known that metallic salts of alkanoates display a complex behavior characterized by the occurrence of several thermal transitions involving crystalline, semicrystalline and liquid-crystalline phases.[11,12] The temperature, nature and number of transitions taking place in these systems are critically dependent on both the length of the alkyl chain and the size of the counter cation.[13] Cholinium alkanoate soaps are in line with the trend observed for metallic alkanoates according to the high voluminosity of the cholinium cation, *i.e.* they adopt a relatively low number of mesophases, and their melting transitions occur at so low temperature that they may be catalogued as ionic liquids.[9] The lyotropic behavior of these systems has been also examined in deep for both short and long alkyl chains.[14]

Surfactants based on fatty acid choline esters are of more recent interest for their potential as suitable components of novel green materials. This class of compounds however has been known for quite some time and shown to display certain biological activity,[15,16] as well as highly appreciated medical properties.[17-21] Long-chain alkanoylcholines are cationic lipids due to the quaternary ammonium functionality in the head-group and they are provided with a high molecular flexibility because the easy rotation of the inserted ester linkage. Although all choline salts are classified as health dangerous compounds just because they are quaternary ammonium ions, a recent toxicity and biodegradability study of choline carboxylate surfactants has proved the innocuity of these products.[22] Alkanoylcholines have in addition the property of being hydrolyzed rapidly by the action of mammalian enzymes to produce fatty acids and choline, both compounds being common human metabolites. This property makes them potentially valuable to replace traditional tetraalkylammonium compounds in personal care products.[23] To our best knowledge, no study addressed to examine the thermotropic properties of alkanoylcholines has been reported to date. Notwithstanding, the Hofmeister anion effect on alkanoylcholines in the hydrated state

has been evaluated as a function of the counter anion for their interest as bioactive surfactants.[24] Although this study was mainly centered in the gel behavior of the whole alkanoylcholine series, the crystal structure of hydrated stearoylcholine iodide was solved. It was reported to consist of a bilayered arrangement with alkanoyl chains aligned and interdigitated in a paraffinic phase that separates the polar layers integrated by the cholinium iodide head groups.

In this paper we study the thermal behavior of the homologous series of alkanoylcholine iodides (nACh·I) derived from lauric, myristic, palmitic and stearic acids (n = 12, 14, 16 and 18, respectively), which are represented in Scheme I. The study examines the thermal transitions occurring in these compounds along the 20-200 °C range both at heating and cooling. The diverse phases appearing or disappearing by effect of temperature are characterized by DSC, real-time XRD, solid-sate ^{13}C CP/MAS NMR and optical microscopy.
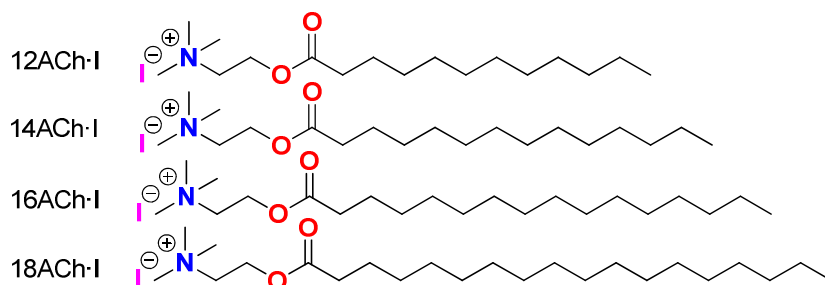
Scheme I. Chemical structure of the alkanoylcholine iodides nACh·I studied in this work (n = 12, 14, 16 and 18).

It is worthy to mention that a good number of studies dealing with the thermal-structural behavior of a wide diversity of cationic surfactants, both in solution and in the pure state, are found in the literature. The occurrence of mesophases of smetic type is a very common feature of all these systems.[11] Among them, the ones closest to the ours are those dealing with tetralkylammonium halides bearing long alkyl groups. In these studies a transition taking place in the 70-130 °C temperature range and leading to a layered semicrystalline structure with the alkyl chains in the molten state was

described. The thermal instability of such compounds hampered the detailed study of high-temperature phases.[25] Attachment of longer alkyl or hydroxyalkyl groups to the nitrogen allowed to observing broad and stable smectic phases.[26]

The alkanoylcholine iodides series object of the present study has been recently used for ionic coupling with microbial poly(γ-glutamic acid) in order to obtain amphiphilic polymeric complexes.[27] These bio-based comb-like polymers are well stable and readily able to self-assemble in supramolecular structures with features similar to the lamellar arrangement described for cationic surfactants bearing long alkyl tails. The thermal transitions taking place in these complexes were found to involve semicrystalline phases and liquid-crystal phases while the thermotropic stuctural behavior of alkanoylcholines has not been examined so far. In addition to contributing to the basic knowledge on choline-based surfactants, the present work was undertaken with the aim of providing the information about alkanoylcholines necessary to evaluate their influence on the structural properties of the complexes that they generate upon coupling to anionic polyelectrolytes.

Experimental

Materials

Lauroyl (98%), miristoyl (97%), palmitoyl (97%) and stearoyl (90%) chlorides, 2-(dimethylamino)ethanol (98%) and methyl iodide (99%) were supplied from Sigma-Aldrich and used as received. Chloroform, dichloromethane, pentane, hexane and acetone were supplied from Panreac and used without further purification.

Synthesis of alkanoylcholine iodides

The synthesis of the alkanoylcholine iodide surfactants (*n*ACh·I) was carried out from 2-(dimethylamino)ethanol, fatty acids of 12, 14, 16 and 18 carbon atoms, and methyl iodide through two concatenated reactions, esterification and quaternization, without isolation of the intermediate aminoethyl ester. The procedure was the following:

A solution of 0.06 mol of 2-(dimethylamino)ethanol (DMAE) in chloroform (50 mL) was added drop-wise to a solution (100 g·L^{-1}) of 0.04 mol of the fatty acid chloride in the same solvent at a temperature between 0 and 20 ºC. After neutralization with aqueous NaHCO$_3$, the organic phase containing the 2-(dimethylamino)ethyl-alkanoate (DMAE-*n*A) was separated as oil. For quaternization, DMAE-*n*A was made to react with an excess of methyl iodide at room temperature. Upon standing overnight the resulting alkanoylcholine iodide (*n*ACh·I) was obtained as a white precipitate that was purified by reprecipitation from chloroform with acetone. Yields were around 90% except for *n* = 12, which was only 25% due to isolation/purification difficulties associated to the higher solubility displayed by this compound. The alkanoylcholine iodides were soluble in a variety of organic solvents such as chloroform, dichloromethane and methanol, and also in hot water. All they were obtained as white powders and their chemical constitution and purity were ascertained by NMR. A detailed account of the conditions used in the synthesis of each compound together with the NMR spectra of the whole series is provided in the ESI file.

NMR

^{1}H- and ^{13}C NMR spectra were registered at 300.1 and 75.5 MHz, respectively, on a Bruker AMX-300 NMR instrument equipped with a variable temperature unit. The samples were dissolved in chloroform and TMS was used as internal reference. 128 FIDs for ^{1}H NMR spectra were recorded with 2.3 μs (30º) pulse width, 3.4 s acquisition time, 20 s relaxation delay, and 4.9 KHz spectral width. For ^{13}C NMR spectra, 1000 to 10000 FIDs were recorded using pulse and spectral widths of 4.3 μs (90º) and 18 KHz, respectively. ^{13}C CP/MAS NMR spectra were recorded within the temperature range of 25 to 95 ºC. Samples were heated first at 190 ºC and then cooled to room temperature before spectral acquisition. Around 200-250 mg sample were spun at approximately 4 KHz in a cylindrical ceramic rotor. All the spectra were acquired with contact and repetition times of 2 ms and 5 s, respectively. Around 640 transients were

accumulated. The spectral width was 31.2 KHz, and the number of data points was 4K. Chemical shifts were externally calibrated against the carbonyl peak of glycine appearing at 176 ppm relative to TMS.

Critical micelle concentration (*cmc*) and Krafft temperature determinations

The *cmc* of *n*ACh·I in D$_2$O was determined by ^{1}H NMR by following the evolution of the chemical shifts of specific signals of the surfactant with increasing concentration according to the procedure described in the literature.[28,29] Samples were dissolved in D$_2$O, and ^{1}H NMR spectra were recorded at the selected temperature using the sodium salt of the 3-(trimethylsilyl)-propanesulfonic acid as internal reference.

The Krafft temperatures were estimated both visually and conductimetrically. For visual estimation, 1% mixtures of *n*ACh·I in water were heated until dissolution and then cooled down to room temperature and kept in a refrigerator at 5 ºC for 24 hours. The cooled samples were then heated up in steps of 1 ºC every 15 min in a water bath provided with a magnetic stirring, and the temperature at which turbidity disappeared was taken as the Krafft temperature. Conductimetry measurements were performed in a Mettler Toledo conductivity meter S30, provided with an Inlab720 sensor with a 0.06 cell constant. Dispersions were heated in a jacketed vessel with a heating rate of 0.5 ºC every 5 min and conductivity was measured. The Krafft temperature was determined as the inflection point of the conductivity values versus temperature plot.

Thermal measurements

Decomposition temperatures (T_d) were measured using a Perkin-Elmer TGA6 thermobalance. Data were collected under a constant nitrogen flow at a heating rate of 10 ºC·min^{-1} within the 30 to 600 ºC temperature interval. Differential scanning calorimetry (DSC) measurements were performed on a Perkin-Elmer Pyris1 DSC instrument provided with an Intracooler device, and calibrated with indium and zinc. Sample weights of about 2-5 mg were examined within a temperature range of -30 to +200 ºC at heating and cooling rates of 10 ºC·min^{-1} under a nitrogen atmosphere.

Several cycles were recorded for each compound and raw data were corrected in order to attain a flat baseline.

X-ray scattering

X-ray real time diffraction studies of powdered samples were carried out using X-ray synchrotron radiation in both WAXS and SAXS modes at the A2 beam-line of light source DORIS III at DESY in Hamburg. Variable temperature experiments were performed at heating and cooling rates of 5 °C·min^{-1}. The energy employed corresponded to a 0.15 nm wavelength, and spectra were calibrated with PET and rat tail tendon for WAXS and SAXS, respectively. X-ray diffraction patterns produced by using conventional light were recorded on the PANalytical X'Pert PRO MPD θ/θ diffractometer using the Cu-K$_\alpha$ radiation of wavelength 0.1542 nm.

Optical microscopy

Optical polarizing microscopy was performed on an Olympus BX51 Orthoplan microscope with an Olympus digital camera attached. A Linkham THMS-600 hot stage provided with a CS-196 nitrogen cooling system, and equipped with TMS90 temperature controller (± 0.5 °C) was used for this study. Thin films of alkanoylcholines were prepared by casting and trapped between glass cover slides. Observations were carried out under a nitrogen atmosphere to avoid contact with air humidity, and at least two heating-cooling cycles were applied for each sample at a rate of 5 °C·min^{-1}.

Stearoylcholine iodide (18ACh·I): single-crystal analysis

Crystallization of 18ACh·I addressed to grow crystals suitable for single-crystal X-ray diffraction analysis was performed by the vapor-diffusion technique. In brief, a solution of 0.5 mg of 18ACh·I in 0.5 mL of chloroform was placed in a capped 2 mL glass vial provided with a needle and the vial put inside a sealed glass flask containing 5 mL of hexane. The solution was then left undisturbed at 25 °C for a few days until a fine crystalline precipitate was observed.

A prismatic crystal (aprox. 0.2 x 0.1 x 0.07 mm) was selected and mounted on a MAR345 diffractometer using graphite monochromatized Mo-Kα radiation (λ = 0.071073 nm) and provided with an image plate detector. Unit-cell parameters were determined from 1141 reflections located in the $3° < \theta < 31°$ range, and refined by the least-squares method. Intensities of 6616 reflections in the range $1.33° \leq \theta \leq 32.32°$ were collected and the structure was solved by direct methods and refined by using SHELXS computer programs. A fully detailed description of the methodology used for this analysis is provided in the Electronic Supplementary Information file (ESI) attached to this paper.

Results and discussion

cmc and T_{Krafft} of *n*ACh·I

The changes taking place at 50 °C in the 3.15-3.30 ppm region of the ^{1}H NMR spectra of 12ACh·I, which is the region in which the resonance of the methyl protons appears, as a function of concentration are depicted in Figure 1a, and the chemical shift of the methyl peak is plotted against the inverse of concentration in Figure 1b. This plot shows that the position of the methyl signal is independent of the amount of surfactant present in the solution until the *cmc* is reached, after which it moves upfield linearly with the inverse of concentration. It is interpreted that below *cmc* the observed resonance signal arises from free surfactant molecules whereas above *cmc* the signal is attributed to the equilibrium mixture of free and aggregated molecules distributed between the solution and the micelles, respectively. The *cmc* values determined by this method for the four *n*ACh·I studied in this work together with the values reported in the literature for the widely known alkyltrimethylammonium bromides (*n*ATMA·Br) are given in Table 1. Note that measuring *cmc* of *n*AChI in water required heating the samples above room temperature to reach the needed concentrations. T_{Krafft} values determined by visual and conductimetric measurements are presented in Table 1. A satisfactory

coincidence was found tetween the two methods. In all cases these temperatures are well above the room temperature and much higher than those reported for nATMA·Br. As it could be anticipated the Krafft temperatures steadily increased with the number of methylenes of the alkyl chain.

Table 1. Values of *cmc* and Krafft temperatures of nACh·I compared with nATMA·Br

Surfactant	T (ºC)	*cmc*	solvent	method	visual	conductimetry
*n*ACh·I						
12ACh·I	50	5.3	D_2O	NMR	38.5	37.9
12ACh·I	80	10.5	D_2O	NMR		
14ACh·I	60	1.9	D_2O	NMR	48.4	50.0
16ACh·I	80	1.0	D_2O	NMR	57.0	55.5
18ACh·I	95	1.2	D_2O	NMR	61.5	61.5
*n*ATMA·Br						
12ATMA·Br	35	16.1[30]	D_2O	NMR	< 0[33]	<0[35]
14ATMA·Br	35	4.1[30]	D_2O	NMR	9.5-10.5[33]	13.2[36]
16ATMA·Br	25	0.9[31]	water	ultrasounds	26[34]	26[37]
18ATMA·Br	40	0.3[32]	water	conductimetry	35-36[33]	-

The header spans: Critical micelle concentration (mM) over T (ºC), *cmc*, solvent, method; and Krafft temperature (ºC) over visual, conductimetry.
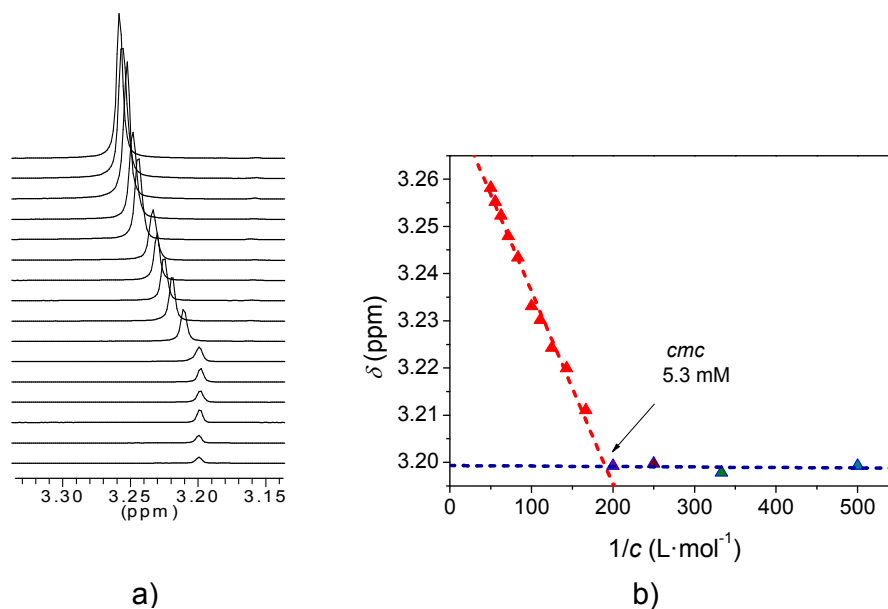

Figure 1. a) Evolution of the ^{1}H NMR methyl signal of 12ACh·I with concentration. b) Plot of the methyl chemical shift against concentration at 50 ºC with indication of the *cmc*.

Thermal decomposition

The TGA traces recorded from nACh·I surfactants under an inert atmosphere are depicted in Figure 2, and the decomposition temperatures together with the weights

remaining after heating at 600 ºC are listed in Table 2. Decomposition of nACh·I was found to start around 200 ºC with onset temperatures increasing slightly with the length of the alkyl chain. TGA derivative curves (see ESI) revealed that the decomposition process evolves trough a mechanism in two-steps that have their respective maximum temperature rates located within the 225-250 ºC and 320-325 ºC intervals. The sample weight loss after the first decomposition step increased steadily from 18% up to 56% with n, whereas no residue was left at the end of the heating treatment. Alkanoylcholines bearing long chains are less thermally stable than acetylcholine in about 30 ºC but compares well to the choline carboxylate soaps,[9] as well as to other cationic surfactants derived from alkylamines.[38]
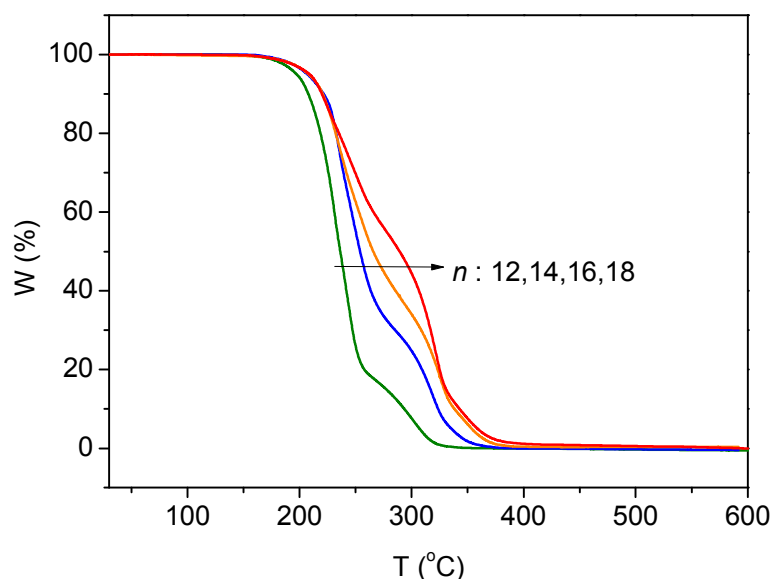

Figure 2. TGA traces of nACh·I recorded under an inert atmosphere.

Differential scanning calorimetry

Since nACh·I compounds start to decompose in the proximities of 200 ºC, the DSC study has been restricted to temperatures below this limit. An exploratory essay in which samples were heated up to 250 ºC did not show any sign of heat exchange in

the 200-250 ºC range. DSC traces of successive heating-cooling cycles of *n*ACh·I

along the 0-175 ºC range of temperatures are depicted in Figure 3, and temperatures

and enthalpies recorded for the thermal transitions observed on first cycle traces are

compared in Table 2. In the four cases, the first heating trace displays a group of two or

three endothermic peaks within the 70-110 ºC interval, in addition to an isolate sharp

peak located between 160 and 170 ºC. The multiple heat adsorption observed in the

lower temperature range strongly suggests the presence of crystal polymorphs that

could be simultaneously generated in the precipitation from solution step that is applied

for purification in the synthesis stage. On the contrary, only two exothermic peaks are

observed on the cooling traces of *n*ACh·I, which are respectively associated to the two

endothermic peaks that are displayed on the second heating traces. These two

exo/endo peak pairs are made to correspond to two reversible transitions taking place

Table 2. Thermal properties of *n*ACh·I surfactants.

nACh·I	TGA[a]			DSC[b]					
				Transition temperatures (ºC) and enthalpies in parenthesis (kJ·mol^{-1})					
				First Heating		Cooling		Second heating	
	$^{o}T_d$ (ºC)	$^{max}T_d$ (ºC)	W (%)	I_{α}/II	II/III	II/I_{β}	III/II	I_{β}/II	II/III
12ACh·I	197	231-243 303	18 0	83 (25.9)	169 (14.2)	41 (-11.3)	165 (-13.8)	52 (10.9)	168 (13.8)
14ACh·I	207	236-247 318	30 0	93 (33.4)	164 (14.6)	47 (-16.7)	161 (-13.0)	59 (15.5)	162 (13.8)
16ACh·I	209	233-254 303	37 0	99 (41.4)	163 (14.6)	59 (-23.0)	160 (-13.8)	70 (22.1)	161 (14.2)
18ACh·I	209	225-247 322	56 0	104 (50.2)	161 (15.0)	70 (-29.3)	157 (-14.6)	80 (24.7)	160 (14.6)
2ACh·I[c]	229	261 322	9 0	165 (32.6)		94 (-24.2)		164 (30.9)	

[a]Onset decomposition temperature at 5% weight lost ($^{o}T_d$), maximum rate decomposition temperature ($^{m}T_d$), and remaining weight (*W*) for each decomposition step.
[b]Transition temperatures and enthalpies recorded at the first DSC run.
[c]Data for this compound refer to its meting/crystallization transition.

in *n*ACh·I along the examined temperature interval. Notice that the transition occurring

in the low temperature region (below 110 ºC) implies a quite large supercooling (~40-

50 ºC) and produces a material that shows at the second heating an endothermic peak at about 30 ºC lower than in the first heating. On the contrary, the high temperature transition is well reproduced in the second heating trace with both position and intensity of the endothermic peak essentially preserved at the initial values. Furthermore, this transition entails a very low supercooling indicating that a very effective nucleation must operate in the recovery of its lower temperature phase. These features strongly suggest that the low temperature exo/endo peaks must involve a crystal melting process whereas the heat exchange taking place at high temperature must arise from a transition implying two structurally close liquid-crystal phases. The DSC recorded from acetylcholine iodide (2ACh·I) (shown in the ESI file) is of valuable help in this regard. The first heating trace of this compound consists of only one sharp endothermal peak at 165 ºC characteristic of melting that is well reproduced in the second heating trace; crystallization at cooling from the melt takes place at about 70 ºC supercooling. The melting peak observed for 2ACh·I is comparable in location to the high temperature transition endothermic peak observed for *n*ACh·I but it entails a much larger enthalpy and its recovery by cooling from the melt requires much larger supercooling. Such dissimilarities clearly indicate that the structural changes implied in each case must be different. Since no liquid-crystal phase is conceivable for the relatively short 2ACh·I molecule, the endothermic peak observed for this compound doubtlessly arises from the melting of the crystal phase into an isotropic liquid phase. On the contrary, heating of *n*ACh·I in the proximities of 160-170 ºC would generate a partially ordered phase where the long amphiphilic molecules still maintain a considerable degree of side-by-side alignment.
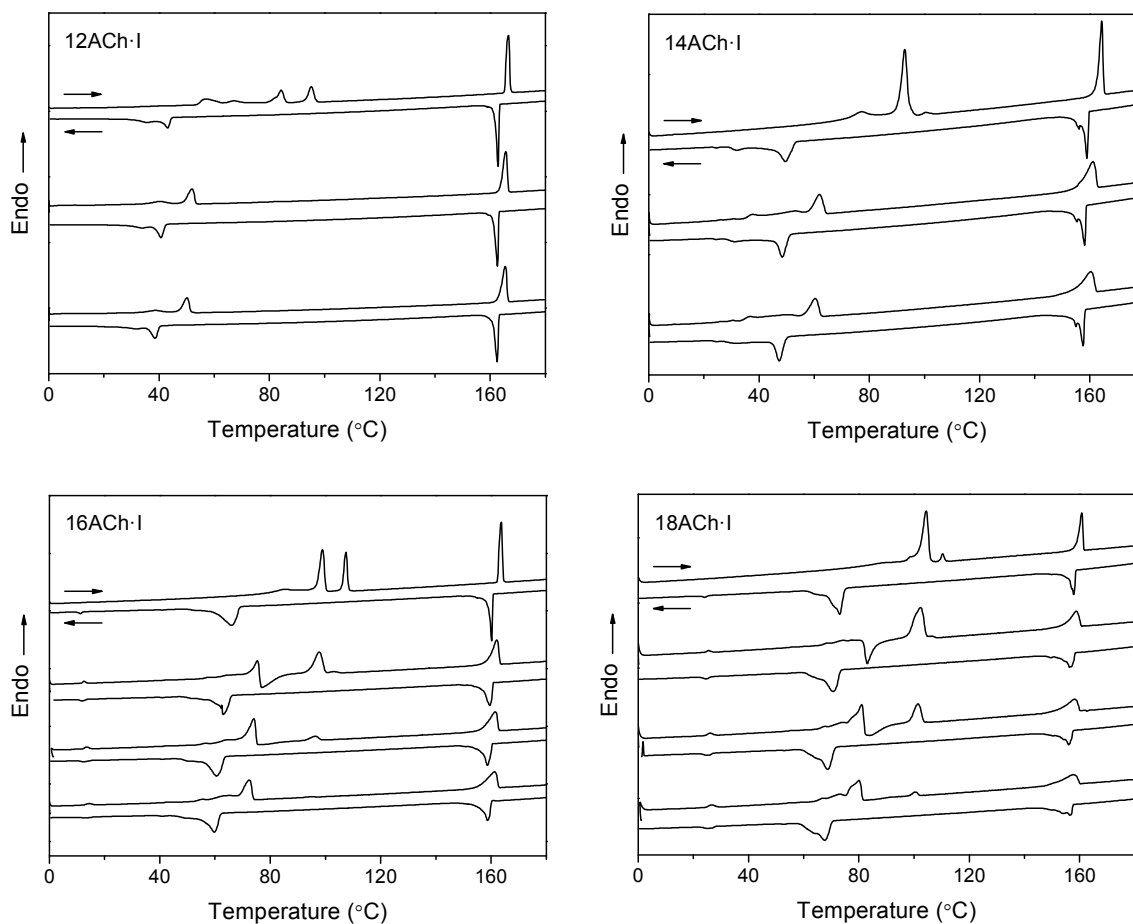
Figure 3. DSC traces of successive heating-cooling cycles (from top to bottom) of *n*ACh·I along the 0-175 ºC range of temperatures.

Coming back to the heat exchange taking place at temperatures below 120 ºC, it should be noticed that the behavior observed for both 18ACh·I and 16ACh·I at the second heating run was different from that displayed by their lower homologues. Both compounds underwent a complex heat exchange process that ended in a material showing an endothermic peak at a temperature similar to that observed for their respective pristine samples. Such pattern is characteristic of a melting-recrystallization process involving a structural rearrangement from a less stable phase to a more stable one. This process however lost relevance with the number of applied heating-cooling cycles. In fact, the initial endothermic peak increased in intensity at the same time that

13

the heat release decreased to fully disappear on the fourth heating trace. It should be stressed that this process was never observed neither for 14ACh·I·nor for 12ACh·I indicating their dependence on the alkyl chain length. The differences between higher (n = 18 and 16) and lower (n = 14 and 12) nACh·I compounds remained for samples that had been previously heated at temperatures below the temperature at which the second transition takes place (160-170 ºC). Furthermore, it was also found that the reverse behavior of 18ACh·I was dependent on the length of time that the sample was maintained under heating. DSC traces demonstrative of this behavior are provided in the ESI document.

At the light of DSC observations and disregarding at this moment the possible polymorphs present in the samples crystallized from solution, four phases may be identified for nACh·I: Two phases (Ph-Iα and Ph-Iβ) with existence at low temperatures, one phase occurring at high temperatures (Ph-III), and one phase with a existence domain in the intermediate temperature region (Ph-II). Ph-Iα is assumed to be a well stable phase formed in the crystallization from solution whereas Ph-Iβ is a metastable phase that is generated by cooling the previously heated samples. Upon standing at room temperature for hours or by annealing, Ph-Iβ is converted in Ph-Iα. The interrelations among these phases are depicted in Scheme II and their structural details are discussed below.
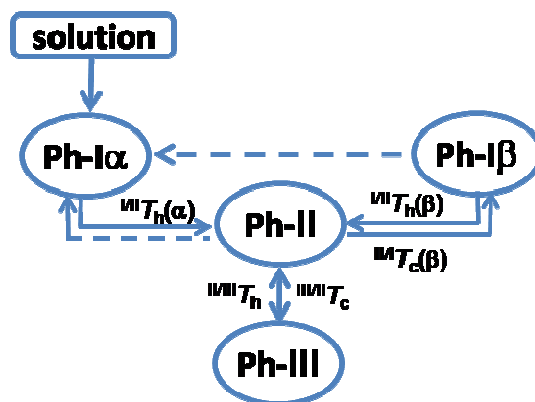
Scheme II. Interrelation between the nACh·I phases and their corresponding transition temperatures (h and c denote heating and cooling).

14

Thermal transitions

Several reversible thermal transitions have been characterized for nACh·I by DSC along the 0-200 ºC interval of temperatures. $^{I/II}T_h(\alpha)$ (measured at the first heating) and $^{I/II}T_h(\beta)$ (measured at the second heating) are the temperatures at which Ph-Iα and Ph-Iβ, respectively, are converted into Ph-II, and $^{II/III}T_h(\alpha)$ is the temperature of conversion of Ph-II into Ph-III. $^{II/I}T_c(\beta)$ and $^{III/II}T_c$ are the temperatures measured on cooling for the Ph-II to Ph-Iβ and Ph-III to Ph-II transitions, respectively. The plot of transition temperatures against n is shown in Figure 4a revealing that a linear trend is followed for all nACh·I although noteworthy differences are observed among them. a) Transitions involving Ph-I and Ph-II take place at temperatures increasing with a similar slope but showing noticeable higher values for $^{I/II}T_h(\alpha)$. b) The supercooling ($^{I/II}T_h(\beta)$ - $^{II/I}T_c(\beta)$) associated to the lower temperature transition is noticeable (around 20 ºC) and essentially constant along the series. c) Both melting and crystallization involving Ph-II and Ph-III occur at temperatures slightly decreasing with n but that are practically coincident along the whole series. The supercooling required for reversing this transition is practically negligible.
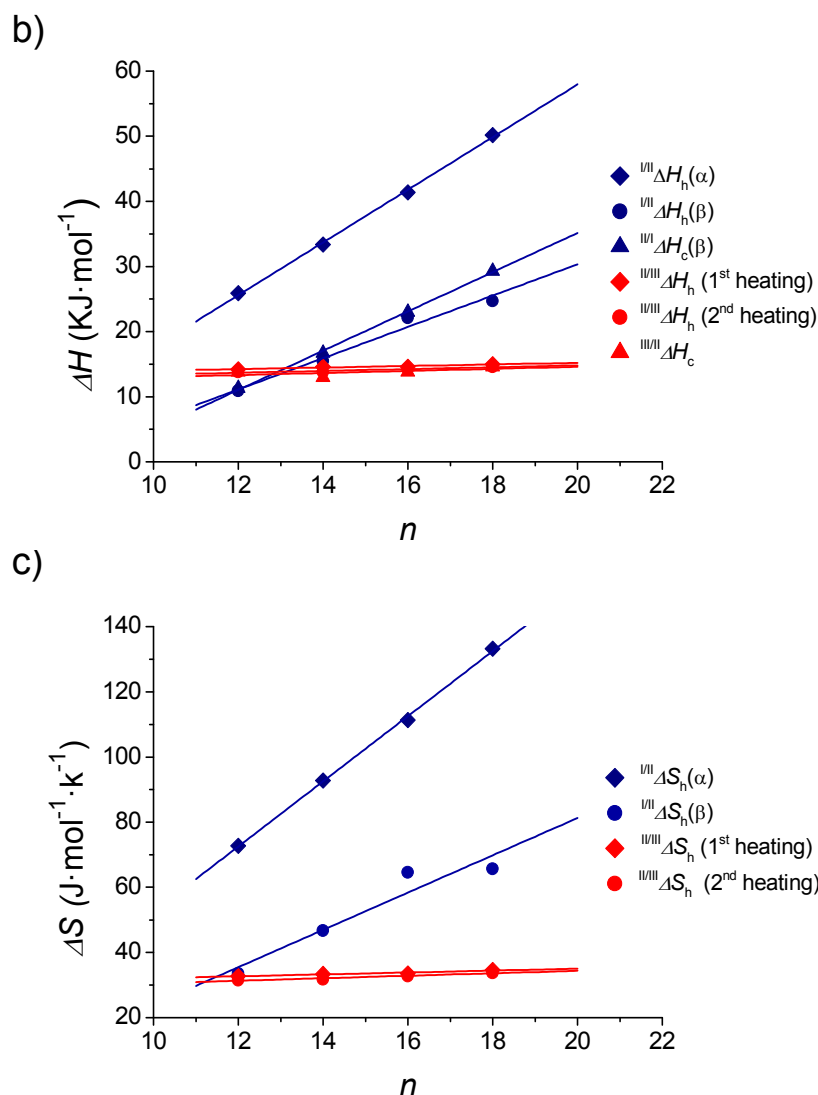
a)

b)

c)
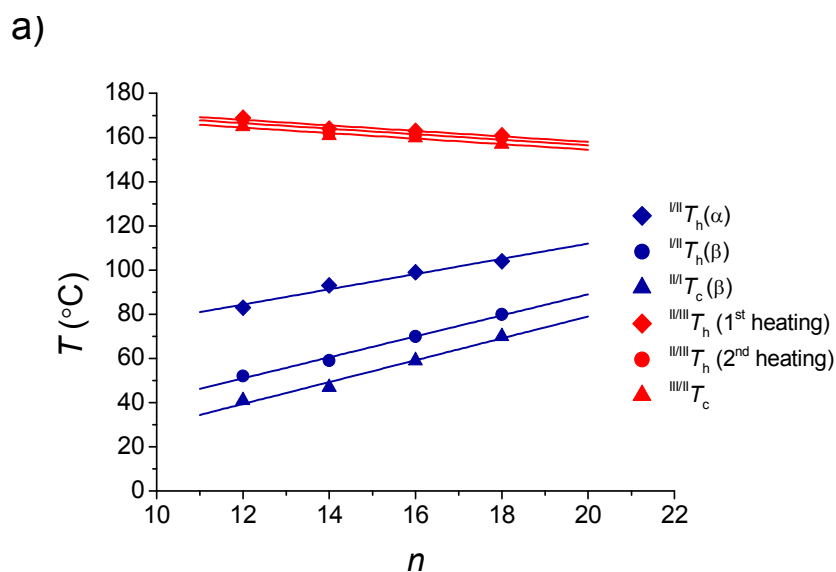
Figure 4. Phase transition temperatures (a), enthalpies (b), and entropies (c) of nACh·I compounds as a function of n. In b) the negative enthalpies registered at cooling are represented in positive values for a closer comparison with the enthalpies registered at heating.

The enthalpy and entropy values involved in the transitions are plotted against n in Figures 4b and 4c, respectively. The values associated to the low temperature transitions increase linearly with n as it should be expected provided that the alkanoyl chain is taking active part in the molecular rearrangement. Moreover the enthalpy associated to the conversion of Ph-Iα into Ph-II (first heating) takes values between 15 and 20 KJ·mol^{-1} higher than for Ph-Iβ, and its variation with n follows a slope of near 25% greater. This is a clear indication of that not only crystallinity of Ph-Iα is higher

16

than of Ph-Iβ but also that the individual methylene contribution to the stability of Ph-I is greater in this phase, as it should be expected for a more efficiently packed crystal phase. With regards to the transition taking place at high temperature, both enthalpy and entropy appear to be practically independent of *n.* This result is fully consistent with the invariability found in both $^{II/III}T_h$ and $^{III/II}T_c$ along the series, and strongly suggests that the alkanoyl chain must not participate actively in the molecular rearrangement involved in this transition.

18ACh·I: A single crystal study

nACh·I were found to yield well shaped microcrystals upon casting from chloroform indicating that the phase Ph-Iα obtained by precipitation from this solvent at room temperature is highly crystalline. Illustrative pictures of the microcrystals made of 18ACh·I are included in the ESI file. With the aim at elucidating in detail the structure present in this phase, a single crystal suitable for X-ray diffraction analysis (0.2 x 0.1 x 0.07 mm size and exempt of significant imperfections such as cracks or twinning) was grown using the vapor-diffusion method in absence of humidity. A picture of the crystal used for the analysis along with a full account of the crystallographic data collected and handled in this study is given in the ESI file. The structure could be resolved with an *R* factor of 0.052. It was found that 18ACh·I crystallized in a triclinic lattice with space group $P\bar{1}$ and unit cell dimensions *a* = 0.576 nm, *b* = 0.767 nm, *c* = 3.09 nm, α = 83.1°, β = 87.0°, γ = 89.3°, containing two molecules related by an inversion centre. A representation of a portion of the crystal lattice including ten unit cells as viewed along the *b*-axis is depicted in Figure 5. In this crystal the stearoylcholine molecules are arranged in a bilayered structure with the polar trimethylammonium iodide head groups arranged along the *C*-plane and the ethyloxystearoyl tails protruding from this plane and following a bended trajectory caused by the kink introduced by the carboxylate unit. As a result the alkyl tails become tilted about 45° respect to the *c-axis* to fix an interlayer distance of ~3.1 nm without appreciable interdigitation. An ORTEP

representation of the 18ACh·I molecule in the conformation adopted in the crystal together with a complete account of their atomic coordinates, bond distances and torsion angles are included in the ESI file.
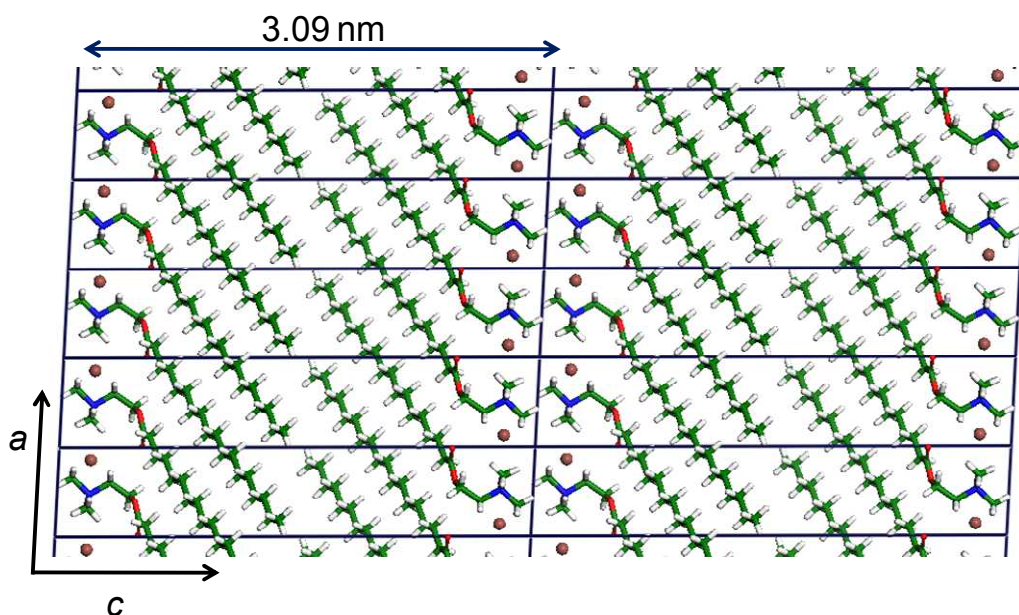

Figure 5. View of the 18ACh·I crystal (Ph-Iα) projected along the *b*-axis. Ten unit cells are visualized.

Tarafdar et al.[24] have recently reported on the crystal structure of 18ACh·I. The structure found by these authors is also triclinic $P\bar{1}$ with unit cell dimensions *a* = 0.799 nm, *b* = 0.963 nm, *c* = 3. 5413 nm, α =86.40°, β = 84.79°, γ = 89.96° and contains 4 molecules. In this structure the alkyl chains are aligned practically parallel to the *c*-axis (tilt angle = 1.7 °) and they are deeply interdigitated. Obviously these authors are dealing with a crystal form of 18ACh·I different from that described above by us. It was noticed that one water molecule every two surfactant molecules was inserted in the crystal lattice described by these authors, which is consistent with the solvent they used for crystal growth (a mixture of chloroform, methanol and water). The presence of water in 18ACh·I could be reasonably invoked to explain the different lattice dimensions found in each case and the consequent difference in the arrangement

adopted by the alkyl chains to fill the interlayer space in the two crystal forms. The critical dependence of the structural behavior of choline-based lipid bilayers on hydration has been accounted in the study of hydrated dihexadecyl phosphatidylcholine in a range of 5-70 wt% of water.[39-41] It was found there that the structure of this compound rearranged from a two-separated sheets bilayer to a deeply interdigitated bilayer at the content in water increased. Different factors including hydrogen bonding were claimed to be responsible for the described water-mediated transition. The amount of water involved in this study is much larger than that adsorbed in the 18ACh·I crystal described by Tarafdar et al.[24]. However the aqueous environment used by these authors used for crystallization could favor initially a hydrated gel interdigitated structure that is retained after most of water is released to form the crystal.

Ph-Iα phase

The WAXS and SAXS profiles recorded from Ph-Iα of nACh·I are compared in Figure 6 for the whole series, and the most characteristic spacings measured on such patterns are listed in Table 3. The samples subjected to this analysis were those coming from synthesis, *i.e.* generated by precipitation from chloroform by adding acetone, after being subjected to annealing in order to improve crystallinity; according to their melting temperatures they consist of Ph-Iα. The presence of a layered structure in these samples is ascertained by the strong reflection appearing in the SAXS region (Figure 6) at a spacing moving from 2.5 nm to 3.1 nm as the alkanoyl chain carbon number increases from 12 to 18. In the WAXS region, all the nACh·I displayed similar patterns consisting of a fair number of sharp peaks concentrated in the 0.50-0.30 nm interval with the strongest one corresponding to the 0.455 nm spacing. Most of the other peaks appearing at lower spacings can be grouped in three groups centered around 0.40, 0.36 and 0.30 nm. The similitude of the groups for the whole nACh·I

series is remarkable with main discrepancies concerning the reflections with $l \neq 0$ as it should be expected from differences in the alkanoyl chain length.

When the XRD pattern experimentally recorded from 18ACh·I powder was compared with the XRD pattern simulated for the crystal structure shown in Figure 5, an extremely close coincidence was found in both SAXS and WAXS regions (see ESI), which confirmed that the structure determined for the monocrystal is that present in Ph-Iα. Furthermore, given the similar scattering displayed by the Ph-Iα phase in all the nACh·I, it can be reasonably assumed that same structure is shared by the whole series. Taking as reference the 18ACh·I crystal structure, similar lattices were built for the other members of the series (see ESI file). The same crystallographic parameters but with the c-axis shortened according to the observed 001 spacing length were used for building, and the same molecular arrangement was maintained in all the cases.
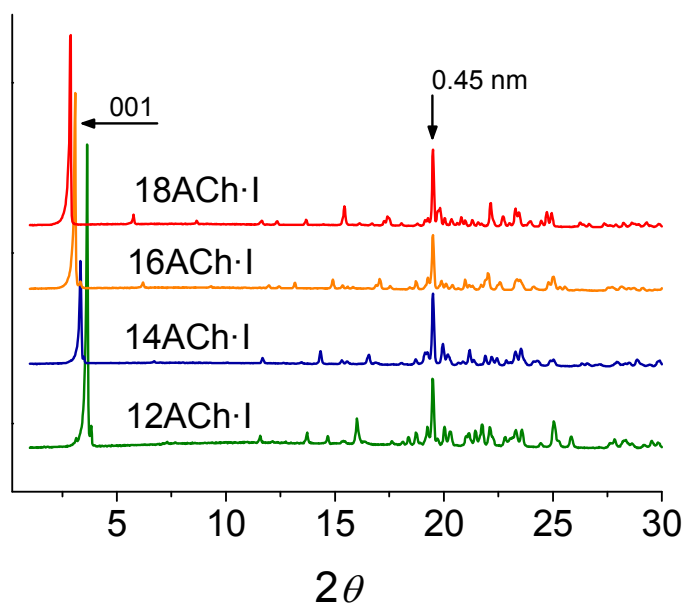

Figure 6. X-ray diffraction profiles of Ph-Iα phase of nACh·I. The peak arising from the intesheet spacing (001) of the layered structure is displayed in the SAXS region ($2\theta < 5°$).The WAXS scattering ($2\theta > 15°$) contains the ~0.45 nm peak characteristic of this phase.

Ph-Iβ, Ph-II and Ph-III phases

Heating of Ph-Iα of *n*ACh·I at temperatures between 80 and 105 ºC led to Ph-II, and further heating of Ph-II above 160-170 ºC led to Ph-III. The exact temperatures at which the phase transitions take place for each surfactant are listed in Table 2. The structural modifications involved in these transitions were followed by X-ray diffraction in real time using synchrotron radiation with simultaneous recording of the scattering changes occurring in the small and wide angle regions. A list of the spacings observed for the whole series in the two regions with precise indication of the temperatures at which they appear is given in Table 3. For illustration the sets of SAXS plots registered from 16ACh·I at heating, cooling and reheating are depicted in Figure 7, and the whole collection of plots recorded from the other members of the series including also those obtained from 2ACh·I are provided in the ESI file.

Table 3. Temperature domains and XRD data for the *n*ACh·I phases.

n	Ph-Iα			Ph-Iβ			Ph-II			Ph-III		
	T (ºC)	SAXS (nm)	WAXS (nm)	T (ºC)	SAXS (nm)	WAXS (nm)	T (ºC)	SAXS (nm)	WAXS (nm)	T (ºC)	SAXS (nm)	WAXS (nm)
12	<83	2.5	0.30 0.36 **0.45**	<52	3.3	0.32 0.35 **0.40** 0.55	52-169	3.5	0.30 0.36 **0.40** 0.55	>169	3.1	-
14	<93	2.7	0.30 0.37 **0.45**	<59	3.6	0.32 0.35 **0.40** 0.55	59-162	3.8	0.30 0.36 **0.40** 0.55	>162	3.3	-
16	<99	2.9	0.30 0.37 **0.45**	<70	4.0	0.32 0.35 **0.40** 0.55	70-161	4.2	0.30 0.36 **0.40** 0.55	>161	3.7	-
18	<104	3.1	0.30 0.37 **0.45**	<103	4.2	0.32 0.35 **0.40** 0.55	103-160	4.5	0.30 0.36 **0.40** 0.55	>160	3.9	-

The strongest reflection observed in each case is in bold

At first glance the two thermal transitions defining the existence domains of Ph-I, Ph-II and III phases are clearly denoted in the SAXS plots by jumps in the positions of their respective characteristic peaks. It is remarkable that whereas Ph-II and Ph-III
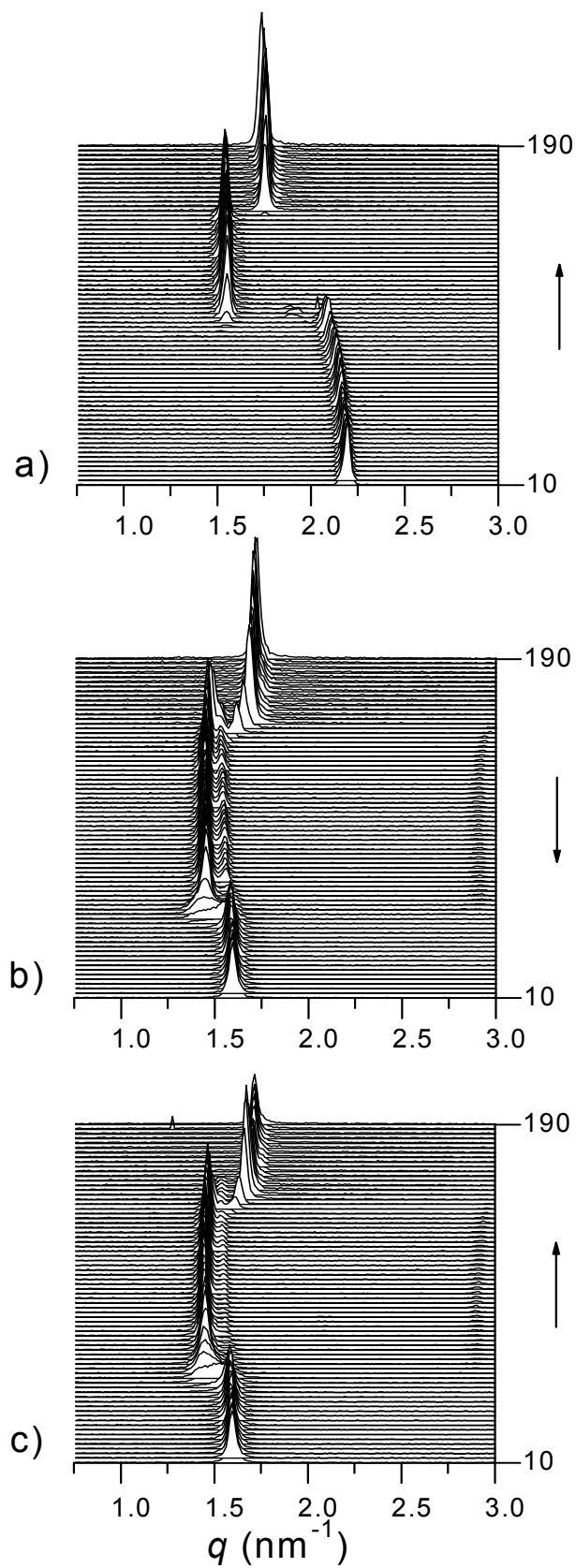
21

Figure 7. SAXS plots from 16ACh·I registered at heating from room temperature (a), cooling (b) and reheating (c).

are faithfully reproduced in second heating plots after cooling, the low-temperature peak (initially Ph-Iα) reappears in the second heating largely displaced towards higher spacings. Furthermore, the three peaks initially observed for 12ACh·I merged into one after cooling from the melt. These results are in concordance with the occurrence of two phases (Ph-Iα and Ph-Iβ) at low temperature, and prove the relative instability of Ph-Iβ respect to Ph-Iα. According to antecedents on other alkylammonium surfactants containing long alkyl chains, the long-spacings observed for nACh·I should be associated to the interlayer distance L characteristic of the lamellar structure present in the crystal, semicrystalline or liquid crystalline phases eventually present in these systems.[25] In fact, no discrete SAXS at all was observed for 2ACh·I as it should be expected from the small acetyl group. The L values for the four phases that have been identified for nACh·I are plotted against n in Figure 8. Remarkable features of this plot are the following: a) A linear trend is obtained for all the phases and extrapolation to n = 0 yields a similar value in the four cases. b) The straight lines resulting for Ph-Iβ, Ph-II and Ph-III are close to each other and have a very similar slope. On the contrary, much lower values of L are found for Ph-Iα and its increment with n occurs at a significant lower ratio.
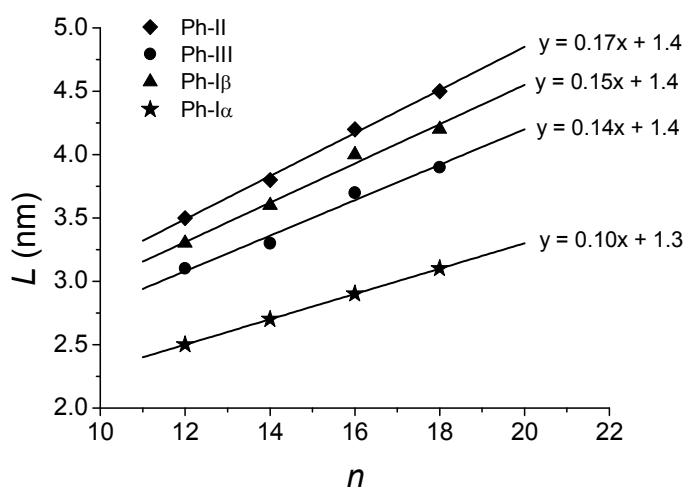

Figure 8. Lamellar interlayer spacing L of nACh·I as a function of the number of carbon atoms in the alkanoyl chain.

A preliminary analysis of the SAXS data taking into account conformational considerations and assuming some approximations regarding molecular volumes allows outlining a first picture of the molecular arrangement present in each phase. First, the difference between the lamellar thickness and the *L*-intercept yields an estimation of the thickness (L_0) of the alkanoyl core in the structure; a comparison of this value with the length of the alkanoyl tail calculated for an *all-trans* conformation (*l*) gives indication of the extent of shortening undergone by the structure in terms of chain tilting, degree of interpenetration or *gauche* conformation present in each phase. The results of these calculations are compared in Table 4. The low $(L-L_0)/l$ ratio (0.8) found for Ph-Iα is consistent with the tilting of the alkanoyl chains and in fully agreement with the crystal model resulting from the structural analysis of the monocrystal. The $(L-L_0)/l$ ratio estimated for Ph-Iβ is between 1.25 and 1.30, which is noticeably higher than for Ph-Iα. Assuming that Ph-Iβ appears as a consequence of the normal orientation respect to the layer plane adopted by the alkanoyl chains upon heating while preserving their fully-extended conformation, the calculated $(L-L_0)/l$ ratio for this phase is consistent with an interdigitated chain arrangement with around 75% of interpenetration. In Ph-II, the $(L-L_0)/l$ ratio is essentially constant along the whole series with a value close to 1.4 according to an interpenetration of 60% provided that both orientation and conformation of the alkanoyl tail are the same as in Ph-Iβ. Regarding Ph-III, the $(L-L_0)/l$ ratio takes values (~1.1) significantly lower than in Ph-II, and even lower than in Ph-Iβ, which reveals a maximum degree of interdigitation for this phase.

Table 4. Interlayer distance *(L)*, choline iodide head size (L_0) and shrinkage ratio $(L-L_0)/l$ in the *n*ACh·I phases.

n [a]	l [b]	Ph-Iα			Ph-Iβ			Ph-II			Ph-III		
		L	L_0	$(L-L_0)/l$	L	L_0	$(L-L_0)/l$	L	L_0	$(L-L_0)/l$	L	L_0	$(L-L_0)/l$
12	1.5	2.5	1.3	0.80	3.3	1.4	1.27	3.5	1.4	1.40	3.1	1.4	1.13
14	1.75	2.7	1.3	0.80	3.6	1.4	1.26	3.8	1.4	1.37	3.3	1.4	1.09
16	2.0	2.9	1.3	0.80	4.0	1.4	1.30	4.2	1.4	1.40	3.7	1.4	1.15
18	2.25	3.1	1.3	0.80	4.2	1.4	1.25	4.5	1.4	1.38	3.9	1.4	1.11

[a] Number of atoms in the alkanoyl tail;
[b] Length of the alkanoyl tail in *all-trans* conformation assuming a C-C bond length of 0.125 nm.

The real-time WAXS analysis of *n*ACh·I afforded invaluable information on the short distance rearrangements, *i.e.* those involving the head groups and alkanoyl tails side-by-side packing, that take place by effect of temperature. The three sets of WAXS profiles registered from 16ACh·I at heating, cooling and reheating are depicted in Figure 9 for illustration, and those recorded from the other members of the series including also those obtained from 2ACh·I, are provided in the ESI file. The spacings of the characteristic peaks of the different phases occurring for *n*ACh·I are listed in Table 3. Inspection of Figure 9 brings to light the following relevant points: a) The initial profiles registered along the first heating run show the peaks characteristic of Ph-Iα, in particular the prominent one at 0.45 nm. b) When temperature overpasses 100 ºC, the profiles become simpler and consist of one main peak located near to 0.40 nm accompanied by two other much weaker peaks at 0.36 and 0.30 nm; this is the pattern characteristic of Ph-II. c) At temperatures above 165 ºC, the scattering losses any vestige of discrete diffraction indicating that Ph-III is fully devoid of crystalline order. Crystallization from Ph-III invariably happens at cooling below 160 ºC with recovery of the WAXS pattern characteristic of Ph-II, which remains essentially unaltered along the whole cooling run finishing at 10 ºC. In fact, no appreciable differences between the WAXS patterns of Ph-II and Ph-Iβ were noticed indicating therefore that the arrangement in the crystalline part of the structure must be the same in the two phases. It seems that differences between Ph-Iβ and Ph-II exclusively concern the periodical repeat of the layered array; according to calculations, it must be the consequence of the different interdigitation degree attained by the alkanoyl tails in each one of these phases.
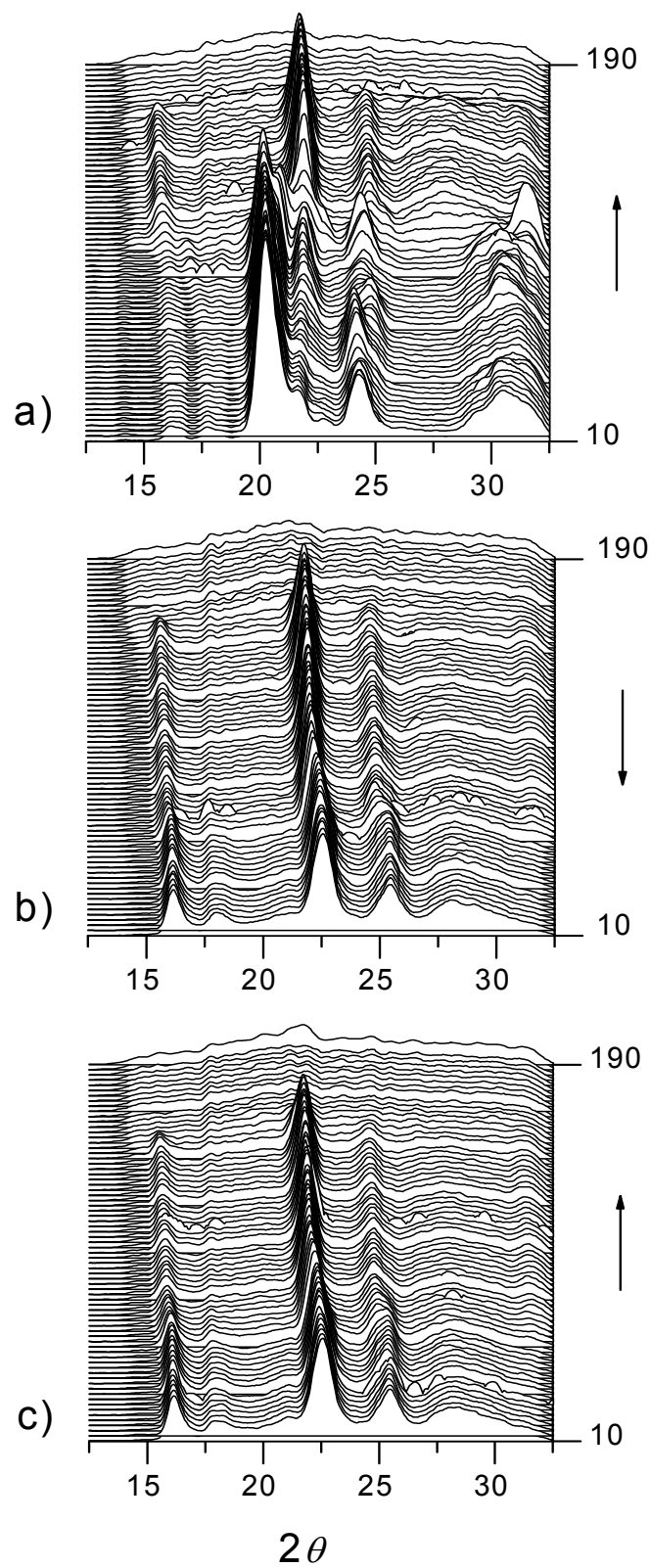
Figure 9. WAXS plots from 16ACh·I registered at heating from room temperature (a), cooling (b) and reheating (c).

26

NMR study of Ph-Iα and Ph-II phases

Additional information of valuable help for the elucidation of the structural changes taking place in *n*ACh·I upon heating was afforded by solid-state ^{13}C CP-MAS NMR. Unfortunately the study of the high temperature interconversion of Ph-II and Ph-III was unfeasible due to limitations in the temperature level attainable by our equipment. The difficulty in the availability of the metastable Ph-Iβ phase in the amounts required for the analysis is an additional shortcoming of this study.

The transition involving Ph-Iα and Ph-II was examined for the whole *n*ACh·I series. Best results were obtained for 12ACh·I because the $^{I/II}T_h$ (α) of this surfactant is well below the maximum temperature allowed by the NMR probe head. All samples subjected to study were initially in Ph-Iα as ascertained by both DSC and WAXS. The spectra recorded from 12ACh·I when subjected to a heating-cooling cycle over the 20-90 ºC interval are reproduced in Figure 10 for illustration, and similar plots for the other members of the series are provided in the ESI document. The changes observed in the signals arising from internal methylene units contained in the alkanoyl chain, as well as those affecting to the carbonyl signal, indicate that the *all-trans* conformation initially present (Ph-Iα) is partially lost when the compound is heated within the 80-90 ºC interval.[42] It is reasonable to interpret therefore that Ph-II consists of a "semicrystalline" phase in which the polar heads of the surfactant are crystallized whereas the alkanoyl tails are side-by-side aligned but without crystalline order. This picture of Ph-II is according to both SAXS and WAXS data and gives strong support to the interpretation of the Ph-Iα to Ph-II transition as a process entailing the melting of the alkanoyl chains accompanied by a slight rearrangement of the ionic pair head groups.

It is worth noting moreover that a change in the NMR signal was perceived in the 14-17 ppm before that Ph-Iα to Ph-II transition takes place. Specifically, the initial alkanoyl methyl signal at 14.5 ppm disappeared upon heating in the 60-70 ºC range, and a peak emerged at around 16.8 ppm instead, which also disappeared when

temperature reached 80 ºC. Such changes are also related to variations in the polymethylene chain packing, and according to observations reported for *n*-alkanes, they must be ascribed to the occurrence of a crystal/crystal transition that is induced by thermal effects.[43]
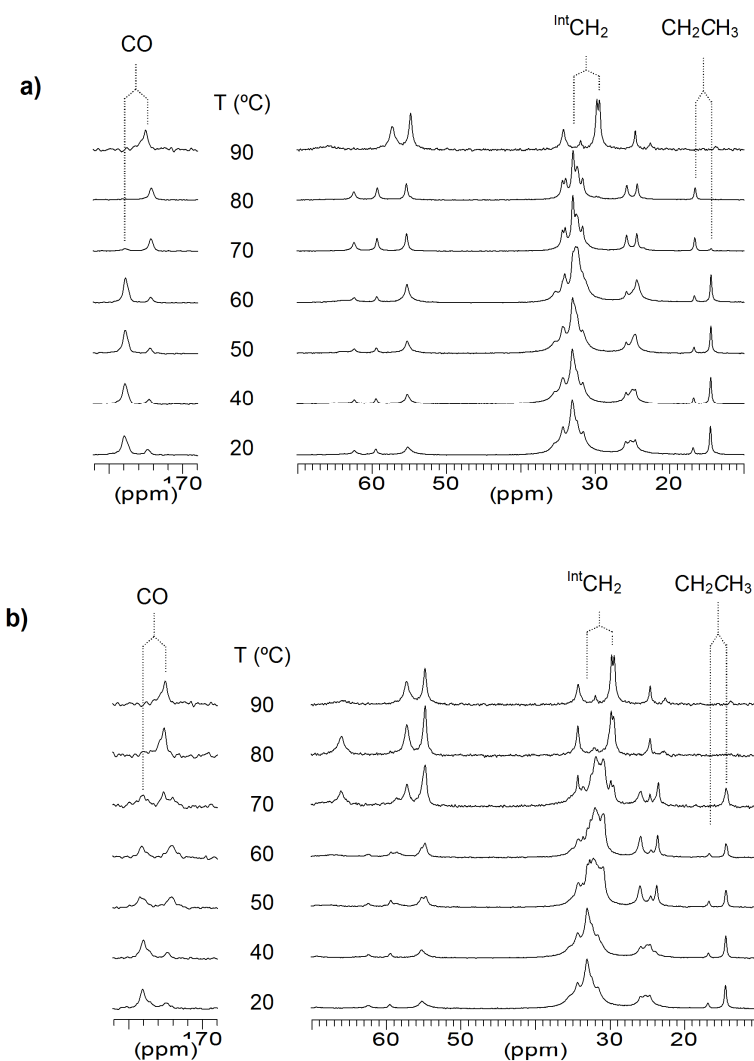

Figure 10. ^{13}C CP/MAS NMR spectra of 12ACh·I registered at the indicated temperatures. a) At heating and b) at cooling.

Polarizing optical microscopy

The thermal transitions taking place in nACh·I were examined by polarizing optical microscopy at both heating and cooling. A selection of the pictures taken from 16ACh·I is shown in Figure 11 and a complete assortment of images illustrating the texture changes occurring in the other members is afforded in the ESI file. Samples for observation were prepared by casting from chloroform at room temperature so they were initially in Ph-Iα phase. The high crystallinity of Ph-Iα previously evidenced by both DSC and WAXS is reflected in the crystal-mosaic texture present in the first pictures taken at low temperatures; this well-defined geometrical morphology was lost after heating above 100 ºC and not recovered any more. The texture seen at 125 ºC corresponds to Ph-II which was observed to evolve with expansion of the material indicating that the Ph-Iα to Ph-II conversion takes place with a decrease in density in agreement with the increase in the interlayer spacing revealed by SAXS. A close inspection of this picture revealed the presence of the features characteristic of a smectic mesophase, which is in full agreement with SAXS results. Further heating at temperatures above ~165 ºC led to Ph-III which displayed a texture not very different from that of Ph-II. In fact, according to WAXS/SAXS data, Ph-II and Ph-III phases will share the same stratified pattern with alkanoyl chains in the molten state intercalated between the layers where the choline iodide counterparts are located. Differences between the two phases concern the order degree of the ionic layer, which is crystallized in Phase II but disordered in Phase III, and the interdigitation degree, which is greater in Phase III. After cooling down to room temperature a strongly birefringent material devoid of any distinctive texture was generated; according to DSC and diffraction data it must correspond to Ph-Iβ, Ph-Iα of even a mixture of both.
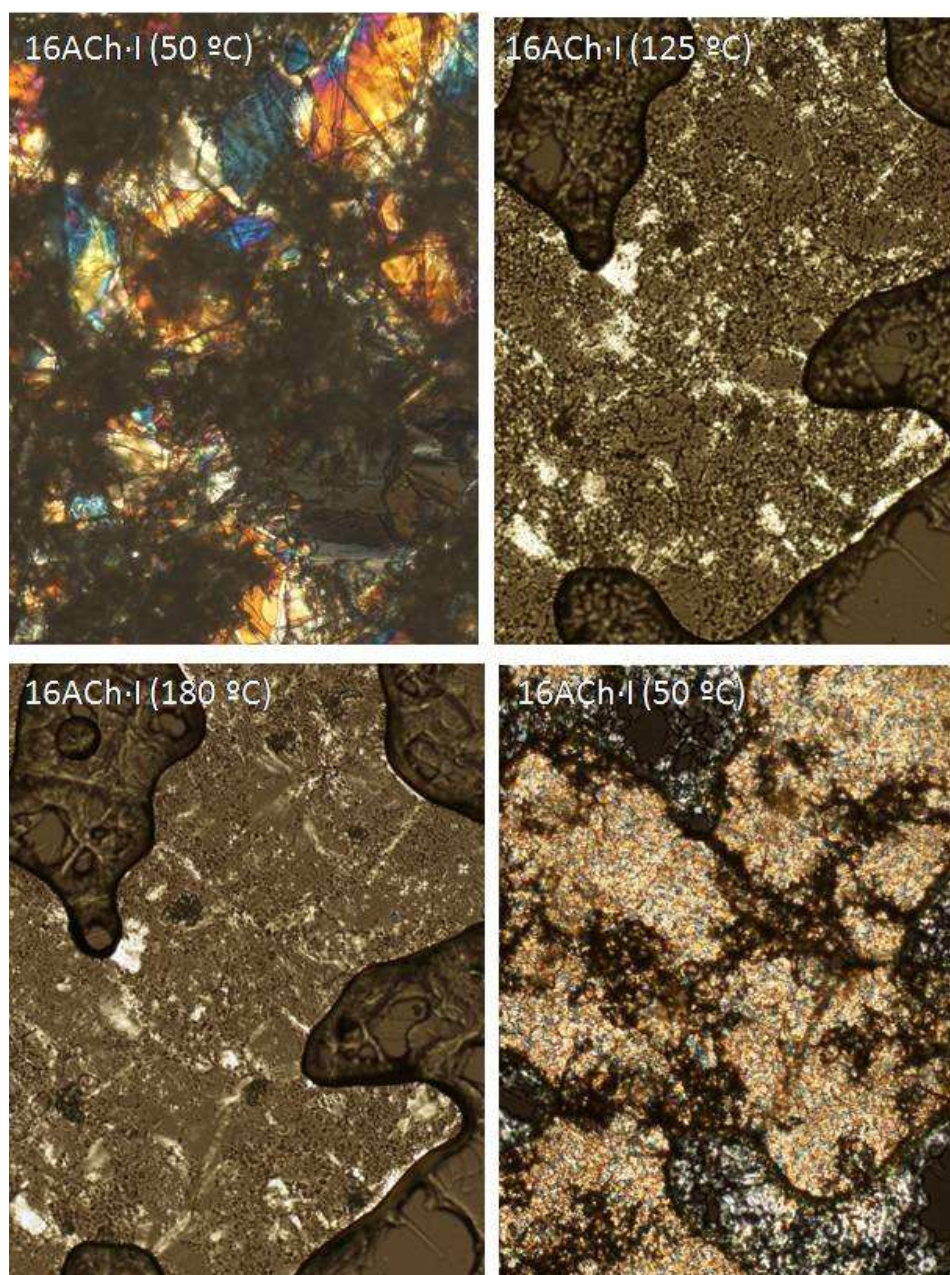
Figure 11. Micrographs recorded by POM from 16ACh·I at the indicated temperatures (the bottom-right one at 50 ºC after cooling).

Conclusions

A homologous series of alkanoylcholine surfactants (nACh·I) has been prepared from fatty acids with n = 12,14,16 and 18, and their thermal and structural properties studied as a function of temperature. These surfactants are particularly interesting

because they are bio-based compounds displaying biodegradable and biocompatible properties, as well as for their suitability to prepare bio-based comb-like polymers by ionic coupling with naturally-occurring polyelectrolytes.

nACh·I surfactants are soluble in warm water showing *cmc* within the 1 to 10 mM concentration range and Krafft temperatures between 30 and 60 ºC depending on n. In the condensed phases, nACh·I invariably adopt a bilayered molecular arrangement in which ionic choline iodide heads and alkyl tails are alternating counterparts. Upon heating, a diversity of phases differing in order degree or/and mutual arrangement of layers are taken up according to temperature. At room temperature, a stable phase (Ph-Iα) made of triclinic microcrystals in $P\overline{1}$ space group prevails whereas at temperatures above 80-100 ºC (depending on n) a semicrystalline layered phase with the alkyl tails in the molten state but aligned and extensively interdigitated is formed (Ph-II). The semicrystalline Ph-II phase becomes fully melted above ~160 ºC with formation of a smectic-A mesophase (Ph-III); in this phase both choline iodide and alkyl tails are in a disordered state but the layered arrangement is still preserved with a higher degree of interpenetration of the alkanoyl chains. The structural changes taking place by heating effect are reversible. Nevertheless a metastable elusive phase (Ph-Iβ) appears when Ph-III is cooled to room temperature; the structure of Ph-Iβ is not well characterized but presumably it is similar to Ph-II but with a degree of side chain interpenetration comparable to Ph-III.
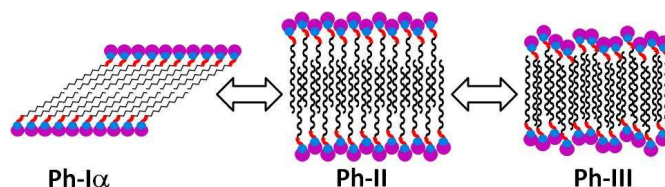

Figure 12. Raw scheme of crystalline, semicrystalline and liquid-crystal phases observed for nACh·I.

Acknowledgements

References

1. J.K. Blusztajn and R.J. Wurtman, *Science,* 1983, **221**, 614-620.

2. J.K. Blusztajn, *Science*, 1998, **281**, 794-795.

3. G.J. Kortstee, *Arch. Mikrobiol*., 1970, **71**, 235-244.

4. J.T. Gorke, F. Srienc and R. Kazlauskas, *Chem Commun*, 2008, 1235-1237.

5. A.P. Abbott, D. Boothby, G. Capper, D.L. Davies and R.K. Rasheed, *J. Amer. Chem. Soc.*, 2004, **126**, 9142-9147.

6. K.D. Weaver, H.J. Kim, J.Z. Sun, D.R. MacFarlane and G.D. Elliot, *Green Chem*, 2010, **12**, 507-513.

7. R. Klein, D. Touraud and W. Kunz, *Green Chem*, 2008, **10**, 433-435.

8. R. Klein, M. Kellermeier, M. Drechsler, D. Touraud and W. Kunz, *Colloids Surf.,* 2009, **338**, 129-134.

9. R. Klein, H. Dutton, O. Diat, G.J.T. Tiddy and W. Kunz, *J. Phys. Chem B,* 2011,**115**, 3838-3847.

10. A. Skoulios and V. Luzzati, *Nature,* 1959, **183**, 1310-1312.

11. K. Binnemans, *Chem. Rev.*, 2005, **105**, 4148-4204.

12. A.R. Ubbelohde, H.J. Michels and J.J. Duruz, *Nature* 1970, **228**, 50-52.

13. K. Shinoda, Y Minegishi and H. Arai, *J. Phys. Chem.* 1976, **80**, 1987-1988.

14. D. Rengstl, O. Diat, R. Klein and W. Kunz, *Langmuir* 2013, **29**, 2506−2519.

15. K.S. Cho and P. Proulx, *Biochim. Biophys. Acta,* 1971, **225**, 214-223.

16. B. Ahlstro m, M. Chelminska-Bertilsson, R.A.Thompson and L. Edebo, *Antimicrob. Agents Chemother.* 1995, **39**, 50-55.

17. R. Schneider and A.R.Timms, *Br. J. Pharmacol.* 1957, **12**, 30−38.

18. V. Carelli, F. Liberatore, L. Scipione, M. Cardellini, D. Rotiroti and V. Rispoli, U.S. Patent 0166721 A1, 2003.

19. H. Patel, W.O. Patent 2005/018631 A1, 2005.

20. J. Alexander and J.A. Fix, U.S. Patent 4,822,773, 1989.

21. J. Alexander, J.A. Fix, and A.J. Repta, J. U.S. Patent 4963556, 1990.

22. R. Klein, E. Müller, B. Kraus, G. Brunner, B. Estrine, D. Touraud, J. Heilmann, M. Kellermeier and W. Kunz, *RSC Adv.* 2013, **3**, 23347-23354.

23. M.K. Watson, U. Tezel, S.G. Pavlostathis, *Water Res.* 2012, **46**, 2947-2956.

24. P.K. Tarafdar, S.T. Reddy and M.J. Swamy, *J. Phys. Chem. B* 2013, **117**, 9900-9909

25. K. Iwamoto, Y. Ohnuki, K. Sawada, M. Seno, *Mol. Cryst. Liq. Cryst.* 1981, **73**, 95-103.

26. A. Malliaris, C. Christias, G. Margomenou-Leonidopoulou, C.M. Paleos, *Mol. Cryst.*

Liq. Cryst. 1982, **82**, 161-166.

27. A. Tolentino, S. León, A. Alla, A. Martínez de Ilarduya and S. Muñoz-Guerra, *Macromolecules* 2013, **46**, 1607-1617.

28. C. Chachaty, T. Ahlnäs, B. Lindström, N. Nery, A.M. Tistchenko *J. Colloid Interface Sci.* 1988, **122**, 406-417.

29. J. Zhao, B.M. Fung *Langmuir* 1993, **9**, 1228-1231.

30. Y.S. Lee, K.W. Woo, *J. Colloid Interface Sci.* 1995, **169**, 34-38.

31. E. Kudryashov, T. Kapustina, S. Morrissey, V. Buckin, K. Dawson, *J. Colloid Interface Sci.* 1998, **203**, 59-68.

32. B.W Barry, G.F.J Russell, *J. Colloid Interface Sci.* **1972**, 40, 174-194.

38. T.W. Davey, W.A. Ducker, A.R. Hayman, J. Simpson, *Langmuir* 1998, **14**, 3210-3213

34. S. Kanehina, H. Matsuki, R. Ichikawa, T. Kuwahara, Proceedings of the International Conference on Colloid and Surface Science, Y. Iwasawa, . Oyama,H. Kunieda Eds., Elsevier, 2001, pp. 45-47.

35. A. Renoncourt, Ph.D dissertation, University of Regensburg, 2005

36. K.S. Sharma, S.R. Patil, A.K. Rakshit, K. Glenn, M. Doiron, R.M. Palepu, P.A. Hassan. *J. Phys. Chem. B* 2004, 108, 12804-12812

37. C. Vautier-Giongo and B. L. Bales, *J. Phys. Chem. B* 2003, 107, 5398-5403.

38 J.A. Portilla-Arias, M. García-Alvarez, A. Martínez de Ilarduya, S. Muñoz-Guerra, *Polym. Degrad. Stab.* **2007**, 92, 1916-1924.

39. M.J. Ruocco, D.J. Siminovitch, R.G. Griffin, *Biochemistry* 1985, **24**, 2406-2411.

40. J.T. Kim, J. Mattai, G.G. Shipley, Biochemistry 1987, **26**, 6599-6603.

41. N.S. Haas, P.K. Sripada and G.G. Shipley, G. G. *Biophys. J.* 1990, **57**, 117-124.

42. T. Yamanobe, M. Tsukahara, T. Komoto, J. Watanabe, I. Ando, I. Uematsu, K. Deguchi, T. Fujito, M. Imanari, *Macromolecules* 1988, **21**, 48-50.

43. D.L. VanderHart, *J. Magn. Reson.* 1981, **44**, 117-125.